

Colour variations in the GRB 120327A afterglow

A. Melandri¹, S. Covino¹, E. Zaninoni², S. Campana¹, J. Bolmer³, B. E. Cobb⁴, J. Gorosabel^{5,*}, J.-W. Kim^{6,27}, P. Kuin⁷, D. Kuroda⁸, D. Malesani⁹, C. G. Mundell^{10,11}, F. Nappo¹, B. Sbarufatti¹², R. J. Smith¹⁰, I. A. Steele¹⁰, M. Topinka¹³, A. S. Trotter^{14,15}, F. J. Virgili¹⁰, M. G. Bernardini^{16,1}, P. D'Avanzo¹, V. D'Elia^{17,18}, D. Fugazza¹, G. Ghirlanda¹, A. Gomboc¹⁹, J. Greiner³, C. Guidorzi²⁰, J. B. Haislip¹⁴, H. Hanayama²¹, L. Hanlon²², M. Im⁶, K. M. Ivarsen¹⁴, J. Japelj²³, M. Jelínek²⁴, N. Kawai⁸, S. Kobayashi¹⁰, D. Kopac²³, A. P. LaCluyzé¹⁴, A. Martin-Carrillo²², D. Murphy²², D. E. Reichart¹⁴, R. Salvaterra²⁵, O. S. Salafia¹, G. Tagliaferri¹, S. D. Vergani²⁶

¹ INAF / Osservatorio Astronomico di Brera, via E. Bianchi 36, I-23807 Merate (LC), Italy

² ICRANet-Rio, Centro Brasileiro de Pesquisas Físicas, Rua Dr. Xavier Sigaud 150, Rio de Janeiro, RJ, 22290-180, Brazil

³ Max-Planck-Institut für extraterrestrische Physik, Giessenbachstrasse 1, D-85748 Garching, Germany

⁴ Department of Physics, The George Washington University, Washington, D.C. 20052, USA

⁵ Instituto de Astrofísica de Andalucía (IAA-CSIC), Glorieta de la Astronomía s/n, 18008, Granada, Spain

⁶ CEOU / Astronomy Program, Dept. of Physics & Astronomy, Seoul National University, Seoul, South Korea

⁷ Mullard Space Science Laboratory, University College London, Holmbury St Mary, Dorking, Surrey RH5 6NT, UK

⁸ Okayama Astrophysical Observatory, National Astronomical Observatory of Japan, Asakuchi, Okayama 719-0232, Japan

⁹ Dark Cosmology Centre, Niels Bohr Institute, University of Copenhagen, Juliane Maries Vej 30, 2100 Copenhagen, Denmark

¹⁰ Astrophysics Research Institute, Liverpool JMU, IC2, Liverpool Science Park, 146 Brownlow Hill, Liverpool L3 5RF, UK

¹¹ Department of Physics, University of Bath, Claverton Down, Bath, BA2 7AY, UK

¹² Department of Astronomy and Astrophysics, Pennsylvania State University, University Park, PA 16802, USA

¹³ Dublin Institute for Advanced Studies, 31 Fitzwilliam Place, Dublin 2, Ireland

¹⁴ Skynet Robotic Telescope Network, Dep. of Physics and Astronomy, Univ. of North Carolina, Chapel Hill, NC 27599-3255, USA

¹⁵ Department of Physics, North Carolina A&T State University, Greensboro, NC 27411, USA

¹⁶ Laboratoire Univers et Particules de Montpellier, Université Montpellier, Place Eugène Bataillon, F-34095, Montpellier, France

¹⁷ INAF / Osservatorio Astronomico di Roma, via Frascati 33, I-00078 Monteporzio Catone (Roma), Italy

¹⁸ ASI Science Data Centre, Via del Politecnico snc, I-00133 Roma, Italy

¹⁹ Centre for Astrophysics and Cosmology, University of Nova Gorica, Vipavska 11c, 5270 Ajdovščina, Slovenia

²⁰ Dipartimento di Fisica, Università di Ferrara, via Saragat 1, I-44100 Ferrara, Italy

²¹ Ishigakijima Astronomical Observatory, NAO of Japan, 1024-1, Arakawa, Ishigaki, Okinawa 907-0024, Japan

²² University College Dublin, School of Physics UCD, Belfield, Dublin 4, Ireland

²³ Faculty of Mathematics and Physics, University of Ljubljana, Jadranska 19, 1000 Ljubljana, Slovenia

²⁴ Astronomical Institute, Czech Academy of Sciences, (ASU CAS), Ondřejov, Czech Republic

²⁵ INAF / IASF Milano, via E. Bassini 15, I-20133 Milano, Italy

²⁶ GEPI, Observatoire de Paris, CNRS, Univ. Paris Diderot, 5 place Jules Janssen, F-92190 Meudon, France

²⁷ Korea Astronomy and Space Science Institute, Daejeon 34055, Korea

Received ; accepted

ABSTRACT

Aims. We present a comprehensive temporal and spectral analysis of the long *Swift* GRB 120327A afterglow data to investigate the possible causes of the observed early time colour variations.

Methods. We collected data from various instruments/telescopes in different bands (X-rays, ultra-violet, optical and near-infrared) and determined the shapes of the afterglow early-time light curves. We studied the overall temporal behaviour and the spectral energy distributions from early to late times.

Results. The ultra-violet, optical, and near-infrared light curves can be modelled with a single power-law component between 200 and 2×10^4 s after the burst event. The X-ray light curve shows a canonical steep-shallow-steep behaviour, typical of long gamma-ray bursts. At early times a colour variation is observed in the ultra-violet/optical bands, while at very late times a hint of a re-brightening is visible. The observed early time colour change can be explained as a variation in the intrinsic optical spectral index, rather than an evolution of the optical extinction.

Key words. Gamma-ray burst: individual: GRB 120327A; ISM: dust, extinction

1. Introduction

The early afterglow is one of most interesting emission stages of Gamma-Ray Bursts (GRBs). In a few tens of seconds the after-

glow emission (X-ray, ultra-violet, optical, infrared and radio) begins to dominate over the fading prompt (gamma-ray) emission, and the time-scale and intensity of the phenomenon offer powerful diagnostics about the physical processes within the outflow and about the environment of the progenitor (e.g. Vestrand

Send offprint requests to: andrea.melandri@brera.inaf.it

* Deceased

et al. 2006; Molinari et al. 2007; Melandri et al. 2008; Liang et al. 2013; Zaninoni et al. 2013).

Of particular interest are those few cases where a colour variation during the early optical afterglow has been singled out (Nysewander et al. 2006; Morgan et al. 2014). GRB 120327A is one of such a few events. In general, early time colour variation can be the signature of rather different phenomena, e.g. the passage of a break frequency of the optical spectrum through the optical bands (e.g. Filgas et al. 2011), variation of the optical extinction due to either dust photo-destruction (Morgan et al. 2014) or the outflow progression through a wind-shaped environment (Rykoff et al. 2004), and also the superposition of different emission stages, such as forward and reverse shock (Kobayashi & Zhang 2003) in the context of the “fireball” model (Piran 2004).

In this paper we report and discuss the observations of the long GRB 120327A, concentrating on the early time colour evolution of the optical light curve. Data are reported in Sect. 2. The results are presented in Sect. 3. The possible interpretative scenarios are discussed in Sect. 4 and conclusions are drawn in Sect. 5. The respective temporal and spectral decay indices α and β are defined by $f_\nu(t) \propto t^{-\alpha} \nu^{-\beta}$, and unless stated otherwise, all errors are reported at 1σ .

2. Observations

GRB 120327A was discovered by the *Swift* satellite (Gehrels et al. 2004) on March 27, 2012, at 02:55:16 UT (Sbarufatti et al. 2012). The bright X-ray and optical counterparts of this long gamma-ray burst ($T_{90} \sim 63$ s; Krimm et al. 2012) were observed by the X-ray Telescope (XRT) and the Ultraviolet and Optical Telescope (UVOT). In the UV it was at $U \sim 18$ a few minutes after the prompt event (Kuin et al. 2012). A redshift was quickly measured by Perley & Tanvir (2012) and Krühler et al. (2012) by absorption lines at $z = 2.813$. Several ground-based facilities observed the field and detected the counterpart in the optical and near-infrared wavelengths. The afterglow was also detected at 34 GHz with a flux density of about 0.7 mJy (Hancock et al. 2012).

In this paper we retrieved and analysed XRT and UVOT data, together with REM telescope (Zerbi et al. 2001; Covino et al. 2004) near-infrared (NIR) data, IAC80, CTIO, BOOTES, PROMPT, Watcher, CQUEAN/2.1m Otto-Struve telescope (Park et al. 2012), GROND (Greiner et al. 2008), SMARTS, MITSuME, NOT, and Liverpool Telescope (LT; Steele et al. 2004) optical data. For the analysis we included also photometric data from LT-RINGO2 imaging polarimeter (Steele et al. 2017). Data are reduced and analysed following standard procedures. Calibration was obtained by means of secondary standard stars in the field provided by the APASS¹ and 2MASS² catalogues in the optical and NIR bands, respectively. R_c and I_c magnitudes have been obtained from APASS r and i magnitudes by means of suitable transformation equations. Optical SMARTS data are calibrated by means of a Landolt standard star field. ZY 2.1m Otto-Struve telescope magnitudes are calibrated following Hodgkin et al. (2009). Optical and NIR magnitudes, not corrected for the Galactic reddening $E_{B-V} = 0.29$ (Schlafly & Finkbeiner 2011), are reported in Table 2 (*Online Material*). These data supersede those published in Kuin et al. (2012), Covino et al. (2012), Gorosabel et al. (2012), LaClyuze et al. (2012), Meehan et al. (2012), Im et al. (2012), Cobb (2012),

Kuroda et al. (2012a,b) and Smith & Virgili (2012). We also used in our analysis data from Sudilovsky et al. (2012).

3. Results

3.1. Light curves

In Fig. 1 the available optical/NIR data are plotted together with the X-ray light curve at 1 keV. The X-ray afterglow shows a canonical steep-flat-steep evolution with a considerable variability superposed on the general trend. The initial X-ray decay ($\alpha_{X,1} \sim 3$) is consistent with the tail of the prompt BAT emission. Between 3×10^2 and 3×10^3 s the light curve flattens to $\alpha_{X,2} \sim 0.4$ and then it becomes steeper to $\alpha_{X,3} \sim 2$ up to the limit of detection.

The optical data start during the X-ray flat phase and show a colour evolution in the optical/NIR afterglow getting redder with time. The evolution is stronger in the bluer bands and more rapid at early-time. We performed a multi-band fit of the UV/optical/NIR data in the time interval $[200, 2 \times 10^4]$ seconds (Fig. 1). Between $10^3 - 10^4$ s the more densely sampled optical bands follow a decay $\alpha_{\text{opt}} \sim 1.2$. To visually emphasise the observed colour variation, in Fig. 2 we normalised all the early time data to the better sampled R -band, shifting all the UBV magnitudes in order to have good accordance at the time $t \sim 10^3$ s (as shown in Fig. 1 the afterglow temporal behaviour after that time is clearly achromatic in the UV/optical/NIR bands). As can be seen the more we move to bluer filters the larger is the deviation at early times from the estimated afterglow decay index. At late time the optical light curve shows the hint of a re-brightening that evolves from the red to the blue. However, the investigation of this late feature is beyond the purpose of this work.

3.2. Spectral energy distributions

For the spectral energy distribution (SED) fit we consider the absorption in the optical and X-ray ranges both locally (i.e., in the GRB host galaxy) and arising from the Milky Way (MW). For the optical band we used the extinction laws given by Pei (1992) (Eq. 20 and Table 4 therein) for the MW, the Large Magellanic Cloud (LMC) and Small Magellanic Cloud (SMC). For the X-ray data, we considered the model for the photoelectric cross section per H-atom units for a given metallicity presented by Morrison & McCammon (1983), assuming solar metallicity (e.g. Covino et al. 2013; Zaninoni et al. 2013).

In addition, D’Elia et al. (2014) showed that the SED of GRB 120327A is characterised by a powerful Lyman $_{\alpha}$ emission with $\log N_{\text{H}} \sim 22$. This implies that the obtained photometry in the bands including hydrogen lines has to be corrected for the line emission. Moreover, some of our data are obtained with filters that cover spectral ranges bluer than the Lyman $_{\alpha}$, i.e. about 460 nm in the observer frame. Together with the host galaxy extinction we therefore need to consider the absorption due to intergalactic-medium that can only be computed in statistical sense. We followed the recipe proposed by Japelj et al. (2012).

In Fig. 3 and Fig. 4 we show the results of the SEDs performed at four different time intervals between 700 and 18000 s after the burst event. The X-ray-to-optical spectral energy distributions are best fitted using a broken power-law³.

We fit the data considering two possible models (Fig. 4):

³A valid solution can still be obtained assuming a single power-law with $\beta_{\text{OX}} \sim 0.85$. However, since the temporal decays in the X-ray and optical bands are different at the time of each SED, this does not seem to be the more plausible solution.

¹<http://www.aavso.org/apass>

²<http://www.ipac.caltech.edu/2mass/>

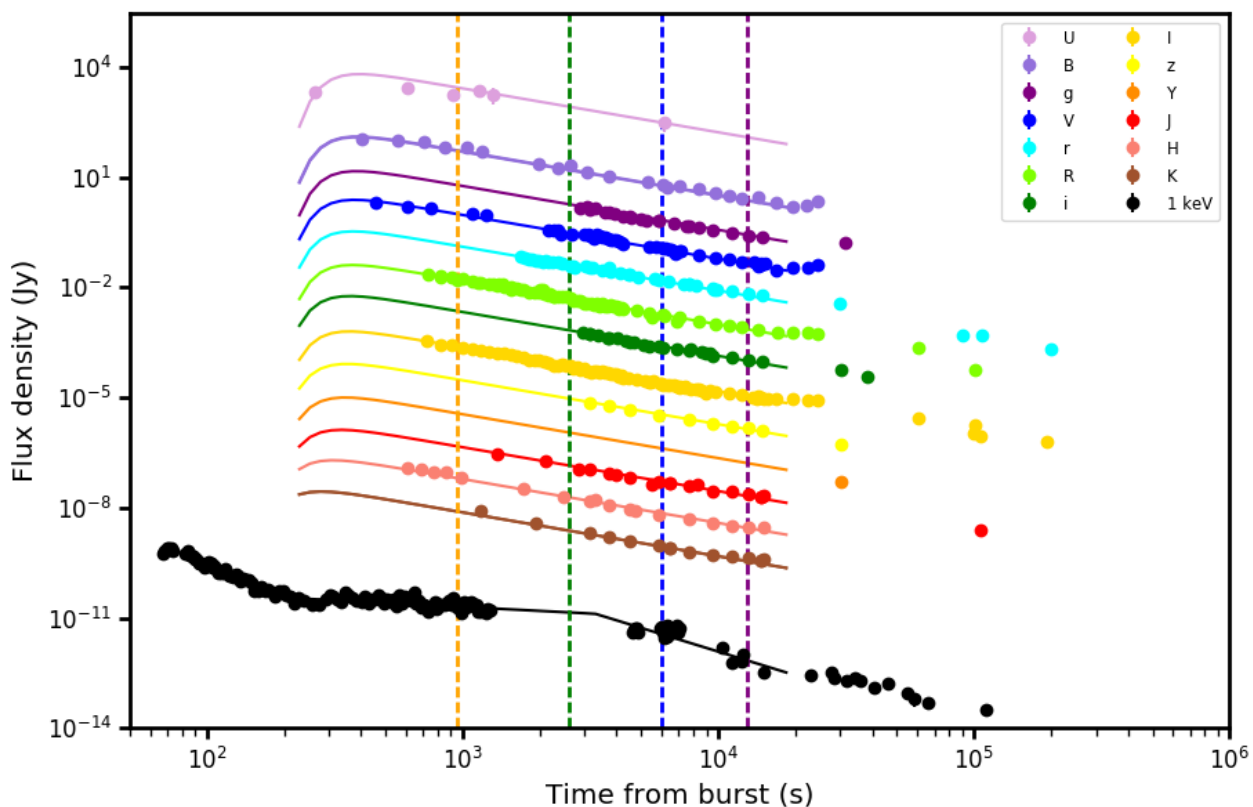


Fig. 1. Optical (UBgVRrIiz), NIR (YJHK) and X-ray (1 KeV) light curve of GRB 120327A afterglow. Bands are artificially shifted for clarity (see Table 2 for calibrated magnitudes). Solid lines represent the best fit for the optical/NIR bands, assuming a variable optical spectral index β and fixed optical extinction. Vertical dashed lines show the T_{mid} of the four SEDs described in the main text.

- Variable optical extinction as $A_V = A_{V0} + k \times t^{0.5}$, with $A_{V0} = 0.04 \pm 0.02$, $k = 6.02 \pm 0.25$ and t the time in seconds from the burst onset⁴; the optical spectral index is constant $\beta = 0.55^{+0.05}_{-0.04}$ (orange area).
- Variable optical spectral index as $\beta = \beta_0 + kt^\alpha$, with $\beta_0 = 0.76 \pm 0.05$, $k = -5.2e5$, $\alpha = -2.34^{+0.23}_{-0.26}$, and t the time in seconds from the burst onset; the optical extinction is constant $A_V = 0.05 \pm 0.02$ (green area).

The data obtained performing the four SEDs (Fig. 3) are in accordance with the second (empirical) model, that is a variable optical spectral index and a constant optical extinction ($\chi^2_{\text{red}} = 1.18$ for 333 d.o.f.). As said before, the X-ray light curve shows the plateau phase between 200 and ~ 3000 s. In this epoch the photon index Γ_X rises from ~ 1.2 at ~ 300 s up to ~ 2.0 at ~ 700 s and then seems to decrease until it sets at the value of $\sim 1.6 \pm 0.1$ (Fig. 4. bottom panel). This is similar to the variation of the optical spectral index, as reported in Table 1 and fitted in Fig. 4 (mid panel), strengthening the validity of our fit with a broken power-law function.

⁴This function is an upgrade of the optical flux attenuation function described by Rykoff et al. (2004), assuming the bulk Lorentz factor Γ of the emitting shell free to vary.

Table 1. Fit parameters of the optical spectral energy distribution at different epochs. ^(a) Without U filter.

T_{min} (s)	T_{max} (s)	T_{mid} (s)	A_V	β
700 ^(a)	1200	950	$0.06^{+0.03}_{-0.03}$	$0.73^{+0.11}_{-0.10}$
1200	4000	2600	0.05 ± 0.03	$0.72^{+0.11}_{-0.09}$
4000	8000	6000	≤ 0.05	$0.81^{+0.08}_{-0.02}$
8000	18000	13000	$0.06^{+0.04}_{-0.03}$	$0.73^{+0.11}_{-0.10}$

4. Discussion

4.1. Early time colour variation

In the context of the standard fireball model (Sari et al. 1998; Chevalier & Li 2000) the GRB afterglow is related to the synchrotron emission from a decelerating relativistic shell that slows into an external medium. The observed colour variation in the optical light curve at early time (Fig. 1 and Fig. 2) could arise from different scenarios:

- (a) the color evolution could be caused by the *passage of a break frequency*. Considering that the spectral index β becomes shallower, the passage of the cooling frequency $\nu_c \propto t^{1/2}$ in the slow cooling wind medium is only the possible case in this scenario, otherwise β becomes steeper or it changes sign (Chevalier & Li 2000). The passage of ν_c is expected to cause the spectral index change $\Delta\beta = 1/2$,

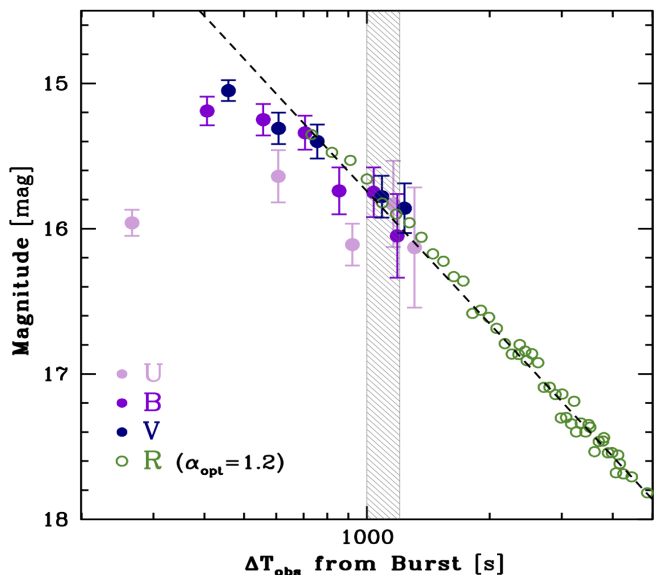


Fig. 2. Early time *UBV* magnitudes normalised to the *R*-band light curve at $t \sim 10^3$ s (shaded region). The dashed line is the power-law decay index of the late time optical afterglow.

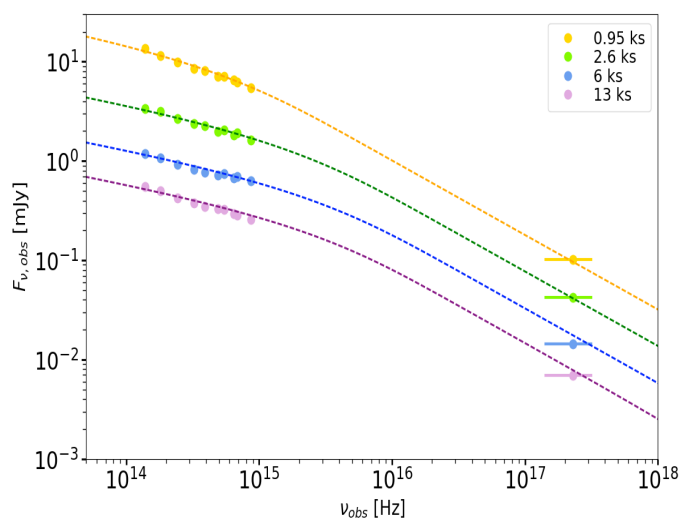


Fig. 3. The four spectral energy distributions estimated at T_{mid} . De-reddened optical data and un-absorbed X-ray flux are shown. Dashed lines represent our fitting model.

simultaneously with the decay index change $\Delta\alpha = 1/4$ in the light curve (Sari et al. 1998). However, the observed change in the spectral index is smaller $\Delta\beta \sim 0.2$ (i.e. the difference in β between the 1st epoch and the later epochs), and no temporal breaks seem to be associated with this spectral change. Moreover, our spectral energy distributions analysis seems to indicate that $\nu_{\text{opt}} < \nu_c < \nu_X$ at the time of each SED (Fig. 3). Therefore the passage of a break frequency can not explain the observations well, and the scenario can be discarded;

(b) the colour change could be simply caused by a *variation of the spectral index* β . Following Morgan et al. (2014), we fit the SEDs letting β free to vary and fixing the dust parameters to the values obtained at late times. Therefore, the colour change can be modelled like a variation in the

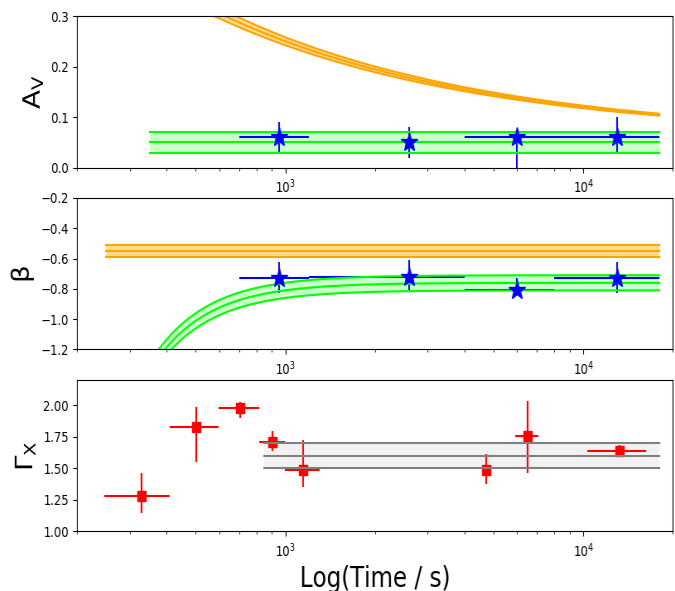


Fig. 4. Evolution with time of the spectral parameters. Variation of the optical extinction A_V (top) and of the optical spectral index β (center). *Blue stars* represent the values obtained by four SEDs as reported in Table 1. *Green area* refers to the model with A_V fixed, while *orange area* to the model with β fixed. *Red squares* (bottom) represent the variation of the X-ray photon index Γ_X , that at late times it settles around the value $\sim 1.6 \pm 0.1$ (gray area).

intrinsic spectral index β , as $F_{\nu_2} = F_{\nu_1} (\nu_2/\nu_1)^{\Delta\beta_{12}}$ (Perley et al. 2010). Indeed, as can be seen in Fig. 4 (middle panel), this possibility could explain the observed data. From our fit, the largest variation of the spectral index is expected at the very early times (green area), where it goes from $\beta \sim -1.4$ at the time of our first UV detection ($\sim 3 \times 10^2$ s) up to $\beta \sim -0.7$ at $\sim 10^3$ s (when in fact the observed temporal behaviour becomes achromatic);

(c) another possible source of the colour variation could be a *change of the optical extinction because of the dust destruction* by the jet within 10 - 30 pc (Draine & Salpeter 1979; Waxman & Draine 2000; Fruchter et al. 2001; Perna & Lazzati 2002; Draine & Hao 2002). This is supported by the fact that long GRBs have massive star progenitors and explode in dusty environments (Morgan et al. 2014). In this case, both the extinction A_V and the reddening R_V are expected to change (e.g. Perna et al. 2003). Therefore, we fitted the optical/X-ray SEDs letting A_V and β free to change, since the dust absorption observed at early times can have different signatures than those at late time (Morgan et al. 2014). For GRB 120327A we do not see a clear variation of the extinction in our spectral analysis. However, we find an excess of the X-ray absorbing column density at early time ($N_{\text{H}} \sim 1.6 \times 10^{22} \text{ cm}^{-2}$) that disappears after ~ 150 s from the burst onset, becoming consistent with the Galactic value (Willingale et al. 2013). Assuming the dust-to-gas relation reported by Covino et al. (2013) this would correspond to an $A_V \sim 1$ mag, implying some sort of extinction variation at very early times. However, the dust destruction scenario seems a contrived explanation.

5. Summary and conclusions

We analysed the temporal and spectral properties of GRB 120327A. The multi-band fit has highlighted the presence of a colour variation from early to late time that cannot be easily explained with the passage of a break frequency through the optical/NIR bands, either with the assumption of an homogenous or wind-like surrounding medium. However, in the fast-cooling case with a wind-like medium, small changes of the spectral index could be the result of the theoretical curvature of the spectrum (Granot & Sari 2006).

No evidence for a change in the absorption A_V (we find an average $A_V = 0.05 \pm 0.02$ for the dust content of the host galaxy), that could explain the observed colour variation, is clearly seen in our data. Although we cannot exclude completely the dust photo-destruction scenario, the variation of the spectral index β seems to be the favoured explanation, reproducing the observed data quite well. Such a variation could be the result of small changes of the microphysical parameters (p , ϵ_e , and ϵ_B) from early to late times. In particular, a small variation of electron spectral index (of the order of ~ 0.4 dex) would reproduce the observed $\Delta\beta$.

Acknowledgements. AM, SCo, SCA, BS, PDA, and GT acknowledge support from the ASI grant I/004/11/3. EZ acknowledges the support by the International Cooperation Program CAPES-ICRANet financed by CAPES - Brazilian Federal Agency for Support and Evaluation of Graduate Education within the Ministry of Education of Brazil. DM acknowledges support from the Instrument center for Danish Astrophysics (IDA). CGM acknowledges support from the Royal Society, the Wolfson Foundation and the Science and Technology Facilities Council. LH acknowledges support from SFI (07-RFP-PHYF295, 11/RFP.1/AST/3188) & the EU-FP7/GLORIA (grant no. 283783). MI and JWK acknowledge the support from the National Research Foundation of Korea grant no. 2017R1A3A3A001362 and no. 2016R1D1A1B03934815. This work has been supported by ASI grant I/004/11/0 and by PRIN-MIUR 2009 grants. This research was made possible through the use of the AAVSO Photometric All-Sky Survey (APASS), funded by the Robert Martin Ayers Sciences Fund. Partly based on observations made with the Nordic Optical Telescope (program 46-003, PI Jakobsson), operated by the Nordic Optical Telescope Scientific Association at the Observatorio del Roque de los Muchachos, La Palma, Spain, of the Instituto de Astrofísica de Canarias.

References

Chevalier R. A. & Li, Z.-Y., 1999, ApJ, 520, L29-L32
 Chevalier R. A. & Li, Z.-Y., 2000, ApJ, 536, 195-212
 Cobb, B. E., 2012, GCN 13188, 1
 Covino, S., et al., 2004, SPIE, 5492, 1613
 Covino, S., Melandri, A., Salvaterra, R., et al., 2013, MNRAS, 432, 1231
 Covino, S., et al., 2012, GCN 13128, 1
 D'Elia, V., Fynbo, J. P. U., Goldoni, P., et al., 2014, A&A, 564, 38
 Draine, B. T. & Hao, L., 2002, ApJ, 569, 780
 Draine, B. T., & Salpeter, E. E., 1979, ApJ, 231, 438
 Filgas, R., et al., 2011, A&A, 535, 57
 Fruchter, A., Krolik, J. H. & Rhoads, J. E., 2001, ApJ, 563, 597
 Gehrels, N., Chincarini, G., Giommi, P., et al., 2004, ApJ, 611, 1005
 Gorosabel, J., Castro-Tirado, A. J., Walker, C., et al., 2012, GCN 13130, 1
 Granot, J. & Sari, R., 2002, ApJ, 568, 820
 Greiner, J.; Bornemann, W.; Clemens, C., et al., 2008, PASP, 120, 405
 Hancock, P., Murphy, T., Gaensler, B., Bell, M., Burlon, D. & de Ugarte Postigo, A., 2012, GCN 13180, 1
 Hodgkin, S. T., Irwin, M. J., Hewett, P. C. & Warren, S. J., 2009, MNRAS, 394, 675
 Im, M., Kim, J.-W. & Kim, D., 2012, GCN 13140, 1
 Japelj, J., Gomboc, A. & Kopac, D., 2012, proc. of Gamma-Ray Bursts 2012 Conference, PoS 078
 Kobayashi, S. & Zhang, B., 2003, ApJ, 597, 455
 Krimm, H. A., et al., 2012, GCN 13137, 1
 Krühler, T., et al., 2012, GCN 13134, 1
 Kuin, P., et al., 2012, GCN 13138
 Kuroda, D., Hanayama, H., Miyaji, T., et al., 2012b, GCN 13169, 1

Kuroda, D., Hanayama, H., Miyaji, T., et al., 2012a, GCN 13156, 1
 LaCluyze, A., et al., 2012, GCN 13127, 1
 Liang, E.-W., Li, L., Gao, H., et al., 2013, ApJ, 774, 13
 Meehan, S., Hanlon, L., Topinka, M. & Kubanek, P., 2012, GCN 13144, 1
 Melandri, A., et al., 2008, ApJ, 686, 1209
 Molinari, E., et al., 2007, A&A, 469, 13
 Morgan, A. N., et al., 2014, MNRAS, 440, 1810
 Morrison, R. & McCammon, D., 1983, ApJ, 270, 119
 Nysewander, M. C., et al., 2006, ApJ, 651, 994
 Park, W.-K., Pak, S., Im, M., et al., 2012, PASP, 124, 839
 Perley, D. A. & Tanvir, N. R., 2012, GCN 13133, 1
 Perley, D. A., Bloom, J. S., Klein, C. R., et al., 2010, MNRAS, 406, 2473
 Perna, R., Lazzati, D. & Fiore, F., 2003, ApJ, 585, 775
 Perna, R., & Lazzati, D., 2002, ApJ, 580, 261
 Rykoff, E. S., et al., 2004, ApJ, 601, 1013
 Pei, Y. C., 1992, ApJ, 395, 130
 Piran, T., 2004, RvMP, 76, 1143
 Sari, R., Piran, T. & Narayan, R., 1998, ApJ, 497, L17
 Sbarufatti, B., et al., 2012, GCN 13123, 1
 Schlafly, E. F. & Finkbeiner, D. P., 2011, ApJ, 737, 103
 Smith, R. J. & Virgili, F., 2012, GCN 13125, 1
 Steele, I. A., Smith, R. J., Rees, P. C., et al., 2004, SPIE, 5489, 679
 Steele, I. A., Kopač, D., Arnold, D. M., et al., 2017, ApJ, 843, 143
 Sudilovsky, V., et al., 2012, GCN 13129, 1
 Vestrand, W. T., et al., 2006, Nature, 442, 172
 Waxman, E. & Draine, B. T., 2000, ApJ, 537, 796
 Willingale, R., Starling, R. L. C., Beardmore, A. P., Tanvir, N. R. & O'Brien, P. T., 2013, MNRAS, 431, 394
 Zaninoni, E., Bernardini, M. G., Margutti, R., Oates, S. & Chincarini, G., 2013, A&A, 557, A12
 Zerbi, F. M., et al., 2001, AN, 322, 275

Table 2. Photometric data used in this paper. Magnitudes are in the Vega system unless for *griz* filters that are in the AB system, and they are all not corrected for Galactic absorption. Errors are at 1σ level.

t-t ₀ (s)	Exp. (s)	Mag	Band	Telescope	t-t ₀ (s)	Exp. (s)	Mag	Band	Telescope
30224	360	19.10±0.02	z	CQUEAN	266	125	17.91±0.09	u	UVOT
3126	177	16.76±0.03	z	GROND	606	39	17.59±0.20	u	UVOT
3728	348	16.98±0.03	z	GROND	921	102	18.06±0.18	u	UVOT
4508	347	17.27±0.03	z	GROND	1162	10	17.78±0.33	u	UVOT
5811	871	17.61±0.03	z	GROND	1308	9	18.08±0.46	u	UVOT
7651	871	17.92±0.03	z	GROND	6166	48	20.01±0.44	u	UVOT
9479	866	18.20±0.03	z	GROND	406	10	16.99±0.11	b	UVOT
11305	873	18.35±0.03	z	GROND	557	10	17.05±0.12	b	UVOT
13134	867	18.49±0.03	z	GROND	706	10	17.14±0.13	b	UVOT
14959	866	18.61±0.03	z	GROND	855	10	17.54±0.18	b	UVOT
30376	360	18.95±0.05	Y	CQUEAN	1038	10	17.55±0.19	b	UVOT
1366	20	14.34±0.04	J	REM	1186	10	17.85±0.32	b	UVOT
2112	246	14.83±0.06	J	REM	6268	48	20.26±0.39	b	UVOT
2859	150	15.41±0.09	J	REM	458	10	15.65±0.08	v	UVOT
3982	300	15.77±0.09	J	REM	608	10	15.91±0.12	v	UVOT
5470	300	16.39±0.15	J	REM	756	10	16.00±0.13	v	UVOT
8341	300	16.43±0.13	J	REM	1088	10	16.38±0.16	v	UVOT
6452	720	16.31±0.07	J	SMARTS	1236	10	16.46±0.19	v	UVOT
14628	720	17.27±0.08	J	SMARTS	6762	48	19.10±0.40	v	UVOT
106377	1800	19.56±0.14	J	SMARTS	2177	10	17.53±0.08	V	PROMPT1
3149	200	16.26±0.05	J	GROND	2263	10	17.56±0.09	V	PROMPT1
3756	376	16.57±0.05	J	GROND	2349	10	17.55±0.08	V	PROMPT1
4535	374	16.82±0.05	J	GROND	2435	10	17.81±0.11	V	PROMPT1
5844	895	17.14±0.05	J	GROND	2659	10	17.76±0.08	V	PROMPT1
7674	895	17.42±0.05	J	GROND	3003	10	17.85±0.08	V	PROMPT1
9503	890	17.75±0.05	J	GROND	3090	10	17.84±0.07	V	PROMPT1
11329	896	17.83±0.05	J	GROND	3158	10	17.85±0.12	V	PROMPT1
13158	891	17.95±0.05	J	GROND	3256	10	18.05±0.08	V	PROMPT1
14982	890	18.11±0.05	J	GROND	3344	10	17.80±0.07	V	PROMPT1
6480	360	16.31±0.07	J	CTIO	3432	10	17.93±0.08	V	PROMPT1
14760	360	17.27±0.08	J	CTIO	3519	10	18.01±0.08	V	PROMPT1
608	50	12.32±0.04	H	REM	3607	10	18.00±0.08	V	PROMPT1
693	50	12.38±0.04	H	REM	3694	10	18.12±0.08	V	PROMPT1
775	50	12.59±0.05	H	REM	3782	10	18.15±0.09	V	PROMPT1
859	50	12.59±0.05	H	REM	3898	10	18.22±0.09	V	PROMPT1
992	150	12.93±0.06	H	REM	3989	10	18.20±0.09	V	PROMPT1
1739	150	13.68±0.06	H	REM	4076	10	18.31±0.10	V	PROMPT1
2485	150	14.33±0.09	H	REM	4164	10	18.35±0.10	V	PROMPT1
3309	300	14.52±0.09	H	REM	4251	10	18.45±0.12	V	PROMPT1
4755	300	15.22±0.15	H	REM	5348	10	18.65±0.04	V	PROMPT1
3149	200	15.91±0.05	H	GROND	6086	10	18.73±0.06	V	PROMPT1
3756	376	16.24±0.05	H	GROND	7078	10	18.94±0.04	V	PROMPT1
4535	374	16.52±0.05	H	GROND	8413	10	19.21±0.05	V	PROMPT1
5844	895	16.87±0.05	H	GROND	9727	10	19.42±0.05	V	PROMPT1
7674	895	17.17±0.05	H	GROND	11056	10	19.47±0.06	V	PROMPT1
9503	890	17.46±0.05	H	GROND	12387	10	19.66±0.07	V	PROMPT1
11329	896	17.63±0.05	H	GROND	14326	10	19.94±0.07	V	PROMPT1
13158	891	17.74±0.05	H	GROND	16927	10	20.24±0.10	V	PROMPT1
14982	890	17.77±0.05	H	GROND	19515	10	20.02±0.08	V	PROMPT1
1179	150	12.30 ± 0.06	K	REM	22302	10	20.02±0.07	V	PROMPT1
1925	150	13.12 ± 0.10	K	REM	24398	10	19.86±0.06	V	PROMPT1
6452	720	14.78±0.09	K	SMARTS	6480	450	18.82±0.03	V	CTIO
14627	720	15.68±0.09	K	SMARTS	14760	450	19.87±0.03	V	CTIO
3149	200	15.61±0.06	K	GROND	5676	225	18.66±0.04	V	SMARTS
3756	376	15.87±0.06	K	GROND	6255	225	18.78±0.04	V	SMARTS
4535	374	16.18±0.06	K	GROND	6540	225	18.86±0.04	V	SMARTS
5843	895	16.48±0.06	K	GROND	7110	225	18.94±0.04	V	SMARTS
7674	895	16.92±0.06	K	GROND	13854	225	19.73±0.04	V	SMARTS
9503	890	17.12±0.06	K	GROND	14427	225	19.84±0.04	V	SMARTS
11329	896	17.21±0.06	K	GROND	14712	225	19.79±0.04	V	SMARTS
13158	891	17.35±0.06	K	GROND	15282	225	19.75±0.04	V	SMARTS
14982	890	17.41±0.07	K	GROND	1993	80	18.72±0.16	B	PROMPT3
6480	360	14.78±0.09	K	CTIO	2351	80	18.98±0.16	B	PROMPT3
14760	360	15.68±0.09	K	CTIO	2625	80	18.80±0.12	B	PROMPT3
656	159	20.43±0.59	uvwl	UVOT	3072	80	19.30±0.18	B	PROMPT3

Table 2. Continued.

t-t ₀ (s)	Exp. (s)	Mag	Band	Telescope	t-t ₀ (s)	Exp. (s)	Mag	Band	Telescope
3740	80	19.54±0.12	B	PROMPT3	3522	10	17.37±0.05	Rc	PROMPT4
5283	80	19.90±0.18	B	PROMPT3	3611	10	17.53±0.06	Rc	PROMPT4
6045	80	20.09±0.23	B	PROMPT3	3700	10	17.46±0.06	Rc	PROMPT4
7054	80	20.24±0.13	B	PROMPT3	3788	10	17.46±0.06	Rc	PROMPT4
8383	80	20.36±0.13	B	PROMPT3	3898	10	17.54±0.07	Rc	PROMPT4
9725	80	20.63±0.15	B	PROMPT3	3986	10	17.54±0.06	Rc	PROMPT4
11060	80	20.87±0.18	B	PROMPT3	4075	10	17.68±0.07	Rc	PROMPT4
12385	80	21.06±0.26	B	PROMPT3	4163	10	17.62±0.06	Rc	PROMPT4
14322	80	20.99±0.17	B	PROMPT3	4252	10	17.69±0.06	Rc	PROMPT4
16926	80	21.31±0.22	B	PROMPT3	5352	10	17.97±0.03	Rc	PROMPT4
19510	80	21.58±0.26	B	PROMPT3	6090	10	18.09±0.04	Rc	PROMPT4
22189	80	21.51±0.27	B	PROMPT3	7087	10	18.28±0.03	Rc	PROMPT4
24351	80	21.24±0.25	B	PROMPT3	8374	10	18.53±0.03	Rc	PROMPT4
2873	30	18.49±0.10	g	Liverpool T.	9735	10	18.71±0.03	Rc	PROMPT4
3080	30	18.44±0.09	g	Liverpool T.	11065	10	18.85±0.04	Rc	PROMPT4
3289	60	18.52±0.06	g	Liverpool T.	12394	10	18.97±0.05	Rc	PROMPT4
3598	60	18.79±0.07	g	Liverpool T.	14347	10	19.08±0.04	Rc	PROMPT4
3916	60	18.90±0.08	g	Liverpool T.	16951	10	19.26±0.04	Rc	PROMPT4
4228	60	19.03±0.08	g	Liverpool T.	19531	10	19.28±0.04	Rc	PROMPT4
4588	60	19.12±0.08	g	Liverpool T.	22304	10	19.26±0.04	Rc	PROMPT4
4972	60	19.25±0.05	g	Liverpool T.	24366	10	19.36±0.06	Rc	PROMPT4
5212	120	19.30±0.05	g	Liverpool T.	100804	10	21.83±0.20	Rc	PROMPT4
5865	180	19.39±0.03	g	Liverpool T.	822	2	15.50±0.06	Rc	Watcher
6733	120	19.54±0.07	g	Liverpool T.	950	2	15.68±0.05	Rc	Watcher
7545	180	19.70±0.04	g	Liverpool T.	1142	2	15.91±0.05	Rc	Watcher
8440	120	19.84±0.05	g	Liverpool T.	1311	2	16.05±0.11	Rc	Watcher
31531	540	20.89±0.07	g	CQUEAN	1375	2	16.02±0.09	Rc	Watcher
3126	177	18.55±0.03	g	GROND	1439	2	16.04±0.11	Rc	Watcher
3728	348	18.78±0.03	g	GROND	1556	2	16.42±0.09	Rc	Watcher
4508	347	19.06±0.03	g	GROND	1684	2	16.34±0.09	Rc	Watcher
5820	871	19.38±0.03	g	GROND	2006	2	16.40±0.12	Rc	Watcher
7651	871	19.69±0.03	g	GROND	2070	2	16.38±0.12	Rc	Watcher
9479	866	19.99±0.03	g	GROND	2198	2	16.69±0.19	Rc	Watcher
11305	873	20.17±0.03	g	GROND	2262	2	16.84±0.24	Rc	Watcher
13134	867	20.34±0.03	g	GROND	2368	30	17.15±0.06	Rc	Liverpool T.
14959	866	20.48±0.03	g	GROND	2465	30	17.26±0.06	Rc	Liverpool T.
732	10	15.35±0.01	Rc	PROMPT4	3010	30	17.49±0.05	Rc	Liverpool T.
821	10	15.47±0.01	Rc	PROMPT4	3218	30	17.54±0.05	Rc	Liverpool T.
912	10	15.53±0.02	Rc	PROMPT4	3494	60	17.70±0.03	Rc	Liverpool T.
1000	10	15.66±0.02	Rc	PROMPT4	3806	60	17.79±0.03	Rc	Liverpool T.
1091	10	15.82±0.02	Rc	PROMPT4	4124	60	17.91±0.03	Rc	Liverpool T.
1180	10	15.90±0.02	Rc	PROMPT4	4454	60	18.06±0.04	Rc	Liverpool T.
1271	10	15.96±0.02	Rc	PROMPT4	4862	60	18.17±0.03	Rc	Liverpool T.
1360	10	16.06±0.02	Rc	PROMPT4	5623	120	18.31±0.02	Rc	Liverpool T.
1451	10	16.17±0.03	Rc	PROMPT4	6392	180	18.49±0.02	Rc	Liverpool T.
1540	10	16.22±0.03	Rc	PROMPT4	7296	120	18.67±0.03	Rc	Liverpool T.
1632	10	16.33±0.03	Rc	PROMPT4	8164	180	18.79±0.02	Rc	Liverpool T.
1722	10	16.36±0.03	Rc	PROMPT4	9616	300	19.01±0.02	Rc	Liverpool T.
1814	10	16.58±0.04	Rc	PROMPT4	9927	300	19.06±0.02	Rc	Liverpool T.
1901	10	16.56±0.03	Rc	PROMPT4	1664	90	16.67±0.05	Rc	Liverpool T.
1990	10	16.61±0.03	Rc	PROMPT4	7650	25	18.66±0.05	Rc	REM
2079	10	16.69±0.03	Rc	PROMPT4	107780	50	22.20±0.10	Rc	REM
2177	10	16.79±0.04	Rc	PROMPT4	90720	1800	22.11±0.15	Rc	NOT
2265	10	16.86±0.04	Rc	PROMPT4	201180	1800	23.06±0.25	Rc	NOT
2352	10	16.87±0.04	Rc	PROMPT4	3438	654	17.50±0.12	Rc	Boote
2441	10	16.84±0.04	Rc	PROMPT4	4104	674	17.65±0.12	Rc	Boote
2537	10	16.86±0.04	Rc	PROMPT4	4812	748	17.82±0.13	Rc	Boote
2626	10	16.92±0.04	Rc	PROMPT4	5520	660	18.24±0.21	Rc	Boote
2714	10	17.09±0.05	Rc	PROMPT4	6186	673	18.17±0.21	Rc	Boote
2803	10	17.09±0.05	Rc	PROMPT4	6858	656	18.59±0.29	Rc	Boote
2898	10	17.14±0.05	Rc	PROMPT4	60769	240	20.34±0.15	Rc	MITSuME
2989	10	17.30±0.06	Rc	PROMPT4	29859	540	20.00±0.02	r	CQUEAN
3078	10	17.30±0.05	Rc	PROMPT4	3126	177	17.56±0.03	r	GROND
3167	10	17.34±0.06	Rc	PROMPT4	3728	348	17.56±0.03	r	GROND
3256	10	17.40±0.06	Rc	PROMPT4	4508	347	18.06±0.03	r	GROND
3345	10	17.34±0.05	Rc	PROMPT4	5820	871	18.39±0.03	r	GROND
3434	10	17.40±0.06	Rc	PROMPT4	7651	871	18.69±0.03	r	GROND

Table 2. Continued.

t-t ₀ (s)	Exp. (s)	Mag	Band	Telescope	t-t ₀ (s)	Exp. (s)	Mag	Band	Telescope
9479	866	18.99±0.03	r	GROND	5561	3600	17.35±0.03	Ic	IAC80
11305	873	19.19±0.03	r	GROND	5945	3600	17.49±0.03	Ic	IAC80
13134	867	19.32±0.03	r	GROND	6319	3600	17.57±0.04	Ic	IAC80
14959	866	19.45±0.03	r	GROND	6700	3600	17.62±0.05	Ic	IAC80
724	10	14.64±0.01	Ic	PROMPT5	7073	3600	17.77±0.04	Ic	IAC80
821	10	14.84±0.02	Ic	PROMPT5	7456	3600	17.71±0.04	Ic	IAC80
911	10	14.88±0.02	Ic	PROMPT5	7829	3600	17.84±0.04	Ic	IAC80
1000	10	15.05±0.02	Ic	PROMPT5	8201	3600	17.90±0.04	Ic	IAC80
1091	10	15.15±0.02	Ic	PROMPT5	8569	3600	17.96±0.06	Ic	IAC80
1181	10	15.27±0.02	Ic	PROMPT5	8942	3600	18.12±0.08	Ic	IAC80
1271	10	15.35±0.02	Ic	PROMPT5	9324	3600	17.94±0.13	Ic	IAC80
1361	10	15.40±0.03	Ic	PROMPT5	2941	30	16.98±0.04	Ic	Liverpool T.
1451	10	15.47±0.03	Ic	PROMPT5	3148	30	17.04±0.04	Ic	Liverpool T.
1541	10	15.51±0.03	Ic	PROMPT5	3389	60	17.15±0.03	Ic	Liverpool T.
1632	10	15.65±0.03	Ic	PROMPT5	3698	60	17.31±0.03	Ic	Liverpool T.
1723	10	15.74±0.04	Ic	PROMPT5	4018	60	17.39±0.03	Ic	Liverpool T.
1814	10	15.96±0.04	Ic	PROMPT5	4328	60	17.54±0.04	Ic	Liverpool T.
1903	10	15.95±0.04	Ic	PROMPT5	4690	60	17.65±0.03	Ic	Liverpool T.
1993	10	15.94±0.04	Ic	PROMPT5	5077	60	17.85±0.05	Ic	Liverpool T.
2082	10	16.02±0.04	Ic	PROMPT5	5374	120	17.88±0.03	Ic	Liverpool T.
2177	10	16.13±0.04	Ic	PROMPT5	6105	180	18.03±0.03	Ic	Liverpool T.
2266	10	16.27±0.05	Ic	PROMPT5	6898	120	18.11±0.03	Ic	Liverpool T.
2355	10	16.32±0.05	Ic	PROMPT5	7779	180	18.14±0.03	Ic	Liverpool T.
2444	10	16.22±0.05	Ic	PROMPT5	8614	120	18.26±0.03	Ic	Liverpool T.
2537	10	16.28±0.04	Ic	PROMPT5	8942	300	18.34±0.02	Ic	Liverpool T.
2626	10	16.33±0.05	Ic	PROMPT5	9254	300	18.41±0.02	Ic	Liverpool T.
2718	10	16.46±0.05	Ic	PROMPT5	38229	900	20.01±0.12	Ic	Liverpool T.
2807	10	16.39±0.05	Ic	PROMPT5	5451	225	17.43±0.04	Ic	SMARTS
2898	10	16.55±0.06	Ic	PROMPT5	6030	225	17.55±0.04	Ic	SMARTS
2987	10	16.48±0.05	Ic	PROMPT5	6881	225	17.71±0.04	Ic	SMARTS
3077	10	16.63±0.05	Ic	PROMPT5	7452	225	17.75±0.04	Ic	SMARTS
3166	10	16.73±0.07	Ic	PROMPT5	13631	225	18.43±0.04	Ic	SMARTS
3256	10	16.69±0.06	Ic	PROMPT5	14203	225	18.54±0.04	Ic	SMARTS
3346	10	16.68±0.06	Ic	PROMPT5	15054	225	18.51±0.04	Ic	SMARTS
3435	10	16.75±0.07	Ic	PROMPT5	15624	225	18.56±0.04	Ic	SMARTS
3524	10	16.70±0.07	Ic	PROMPT5	99214	2160	20.92±0.05	Ic	SMARTS
3614	10	16.80±0.07	Ic	PROMPT5	106376	2160	21.07±0.06	Ic	SMARTS
3704	10	16.74±0.06	Ic	PROMPT5	193116	2160	21.45±0.07	Ic	SMARTS
3793	10	16.88±0.08	Ic	PROMPT5	6480	450	17.63±0.04	Ic	CTIO
3898	10	16.84±0.06	Ic	PROMPT5	14760	450	18.47±0.04	Ic	CTIO
3988	10	16.90±0.07	Ic	PROMPT5	60769	2640	19.84±0.34	Ic	MITSuME
4078	10	17.01±0.08	Ic	PROMPT5	30079	360	19.55± 0.01	i	CQUEAN
4167	10	16.95±0.07	Ic	PROMPT5	3126	177	17.07±0.03	i	GROND
4259	10	17.11±0.08	Ic	PROMPT5	3728	348	17.30±0.03	i	GROND
5354	10	17.39±0.04	Ic	PROMPT5	4508	347	17.59±0.03	i	GROND
6093	10	17.61±0.05	Ic	PROMPT5	5820	871	17.92±0.03	i	GROND
7049	10	17.67±0.04	Ic	PROMPT5	7651	871	18.23±0.03	i	GROND
8378	10	17.89±0.04	Ic	PROMPT5	9479	866	18.52±0.03	i	GROND
9698	10	18.07±0.04	Ic	PROMPT5	11305	873	18.67±0.03	i	GROND
11029	10	18.17±0.05	Ic	PROMPT5	13134	867	18.83±0.03	i	GROND
12372	10	18.28±0.05	Ic	PROMPT5	14959	866	18.96±0.03	i	GROND
14394	10	18.40±0.04	Ic	PROMPT5	807	2	15.53±0.09	C	Watcher
16927	10	18.58±0.04	Ic	PROMPT5	810	2	15.34±0.09	C	Watcher
19540	10	18.54±0.04	Ic	PROMPT5	814	2	15.48±0.08	C	Watcher
22342	10	18.61±0.04	Ic	PROMPT5	1091	30	15.93±0.58	C	Watcher
24369	10	18.68±0.05	Ic	PROMPT5	1387	30	15.94±0.36	C	Watcher
100848	10	20.33±0.12	Ic	PROMPT5	1568	30	16.45±0.64	C	Watcher
4425	3600	17.12±0.03	Ic	IAC80					
4809	3600	17.21±0.03	Ic	IAC80					
5183	3600	17.30±0.03	Ic	IAC80					